IEEE Access
Multidisciplinary ⋮ Rapid Review ⋮ Open Access Journal

Received 28 May 2024, accepted 13 July 2024, date of publication 18 July 2024, date of current version 1 August 2024.

Digital Object Identifier 10.1109/ACCESS.2024.3430309

RESEARCH ARTICLE

Research on Automatic Bleeding Detection in Arthroscopic Videos Based on Composite Color and Statistical Features

ZEWEN LIU[1,2], XIANCHENG WANG[1], YI YUAN[3], RUIDONG LI[1,2], AND WENPING XIANG[1,2]

[1]College of Science and Technology, Ningbo University, Ningbo 315300, China
[2]Faculty of Mechanical Engineering and Mechanics, Ningbo University, Ningbo 315211, China
[3]The Second Hospital of Ningbo, Ningbo 315010, China

Corresponding author: Xiancheng Wang (wangxiancheng@nbu.edu.cn)

This work was supported by the Horizontal Research Program of the College of Science and Technology of Ningbo University under Grant HXSP2023122801.

This work involved human subjects or animals in its research. Approval of all ethical and experimental procedures and protocols was granted by the Institutional review board (IRB) of Ningbo Second Hospital.

ABSTRACT Arthroscopic surgery is a primary technique for treating joint-related diseases, widely embraced in clinical practice for its minimally invasive and precise nature. However, intraoperative bleeding often generates blood mist, significantly impairing the surgeon's field of view and necessitating prompt high-flow drainage for clearance. Therefore, accurate bleeding detection and localization is a prerequisite for blood mist removal. This paper introduces a pixel-based feature extraction scheme aimed at detecting bleeding frames in arthroscopic videos. In contrast to previous bleeding detection methods, this approach utilizes statistical features based on composite color to analyze arthroscopic images and extract features. Then, a feature selection strategy is proposed to select the best features from the extracted features.Subsequently, the selected features are fused and then classified using an improved KNN classifier to differentiate between bleeding and non-bleeding images. In addition to this, a post-processing scheme is introduced to enhance bleed frame detection performance by exploiting temporal variations across consecutive frames in arthroscopic videos. Lastly, a region-based detection algorithm is proposed for identifying bleeding zones within images depicting bleeding. By conducting extensive experimental analysis on the arthroscopic image and video dataset. The proposed method achieves accuracies of 95.8%, 97.3%, and 95.3% for bleed frame detection in terms of accuracy, sensitivity, and specificity respectively. The results demonstrate that the proposed algorithm effectively detects bleeding frames and bleeding zones in arthroscopic videos.

INDEX TERMS Arthroscopy surgery, bleeding detection, bleeding zones, composite color, statistical features.

I. INTRODUCTION

Arthroscopy is a medical technique utilized for intra-articular examination. It involves the insertion of a slender instrument into the patients' joint cavity for visualization. Arthroscopic surgery minimizes the need for extensive incisions associated with conventional open procedures, thereby mitigating surgical trauma, pain, and recovery duration. Effective management of bleeding, especially during surgery, has a significant impact on patient safety and recovery. Bleeding can result in impaired visibility and compromise surgical results, while excessive bleeding may pose significant health risks to those patients. Hence, precise and prompt detection of bleeding during arthroscopic procedures, coupled with meticulous hemostasis, significantly enhances surgical outcomes and ensures patients safety.

Compared with the wireless capsule endoscopes, the two kinds of arthroscopes employ endoscopic technology, and

The associate editor coordinating the review of this manuscript and approving it for publication was Wu-Shiung Feng.

during the procedure, images or videos are captured by an internal camera, which allows doctors to observe the patients' bodies in the real time. However, relying only on the naked eye for a long period of time will inevitably lead to large results errors. As a result, several attempts have been undertaken in recent years by researchers from various nations to identify bleeding in wireless capsule endoscopy images or videos. Various algorithms and techniques have been developed with the aim of improving the accuracy and efficiency of testing. Those efforts have not only significantly improved the quality of medical diagnosis, but reduced the workload of doctors and advanced the development of smart medical technologies. Charfi and Ansari [1] and Pannu et al. [2] utilized the HSV color space along with a supervised learning ensemble for the detection of bleeding in endoscopic images respectively. Garcia-Martinez et al. [3] proposed a computer vision algorithm for bleeding detection following the classification of pixels in each image frame into bleeding and background pixels. Ghosh et al. [4], [5], [6] respectively proposed a pixel-based overall feature extraction method, a block-statistic color histogram-based automatic video bleeding detection method as well as a deep learning-based semantic segmentation method for detecting bleeding zone in endoscopic images. In contrast, Kundu and Fattah [7] and Pogorelov et al. [8] proposed a local feature extraction method from pixels of interest in endoscopic images based on feature probability density function fitting and an automated bleed detection technique based on color and texture features respectively. For the classification purposes, this article in [9] proposed a machine learning technique on the basis of supporting vector machines in which all pixels in an image are classified as either bleeding or non-bleeding pixels based on its color features. Liaqat et al. [10] proposed a feature selection strategy based on HSV color transform to extract geometric features from CE images and classify bleeding images. Hajabdollahi et al. [11] chose suitable color channels as inputs for the neural network, employing both multilayer perceptron (MLP) and convolutional neural network (CNN) for images classification respectively. Caroppo et al. [12] introduced a novel computer-aided diagnostic system designed for the automatic classification of endoscopically acquired images into images with lesions and lesion-free images. Rustam et al. [13] and Usman et al. [14] developed a deep neural network and a video frame classification model using SVM for classifying bleeding frames in CE videos respectively. In addition to that, in some studies in recent years, different researchers have again taken different approaches on bleeding detection. Rathnamala and Jenicka [15] proposed an automated system based on Gaussian Mixture Model Hyperpixel for the detection and segmentation of candidate zones for bleeding. Caroppo et al. [16] proposed an approach utilizing three pre-trained deep Convolutional Neural Networks for features extraction. Subsequently, a supervised machine learning algorithm is applied to classify the extracted features into bleeding and non-bleeding images for bleeding detection. Rani et al. [17] introduced a novel automated method for bleeding detection in endoscopic images by integrating three pre-trained CNNs: InceptionV3, ResNet152V2 and InceptionResNetV2. Alam et al. [18] proposed a convolutional neural network-based architecture that effectively leverages region information and attention mechanisms for the classification of anomalies in endoscopic video data. Lu et al. [19] presented a method for extracting and fusing multi-scale deep features for detection and localization. Another paper in [20] introduced a machine learning technique for detecting bleeds and zones in endoscopy videos and ultimately localizing the bleeding zones on the basis of appropriate fusion methods and thresholds.

In the previous studies, most of them have basically only conducted various studies such as bleeding detection on videos or images taken by capsule endoscopes, while there are basically zero studies on bleeding detection under arthroscopic surgery, in order to solve the problem.This paper presents a method to identify and precisely localize bleeding zones using video footage during arthroscopic surgery. Video identification enables real-time monitoring of bleeding during surgery, allowing precise localization of the bleeding zone using an algorithm. This approach enables surgeons to gain a comprehensive understanding of bleeding dynamics throughout their surgical procedures, facilitating informed adjustments to surgical strategies and preparation of requisite instruments and medications. The main contribution of this paper is:

1) This paper proposes an automatic detection method for bleeding frames and bleeding zones in arthroscopic videos, which provides some assistance in accurately identifying bleeding during arthroscopic surgery.

2) This paper presents an improved KNN algorithm, which offers better accuracy for bleeding detection in arthroscopic images compared to traditional KNN algorithms.

3) This paper introduces a post-processing algorithm which significantly improves the classification performance of arthroscopic images.

Overall, this study provides some insights into the identification of bleeding during arthroscopic surgery and provides a valuable reference for surgeons to accurately eliminate the interference of bleeding in surgery. This largely reduces the interference of bleeding to the surgeon during surgery, which in turn shortens the operation time, reduces the difficulty of the operation, and improves the safety and precision of the operation.

II. METHODS

Figure 1 displays the suggested method's flowchart. Firstly, frame-by-frame extraction occurs from a provided arthroscopic video stream. Secondly, the extracted frames undergo preprocessing, followed by feature extraction upon transforming the RGB color space into the R/G color plane. Subsequently, the extracted features are fused after feature selection, and next, a KNN classifier is used to distinguish between bleeding images and non-bleeding images. Lastly,

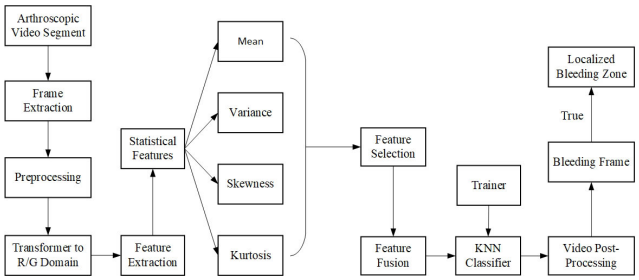

FIGURE 1. Diagram showing the suggested methods work flow chart.

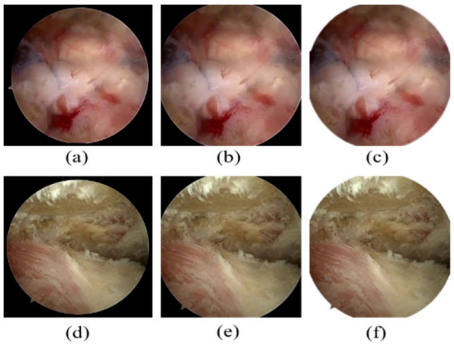

FIGURE 2. Example of preprocessing steps: (a) Original frame with arthroscopic bleeding; (b), (e) After eliminating the rectangular black part; (c), (f) The final preprocessed image following the removal of the black regions in the corners; (d)Arthroscopic non-bleeding Original Frame.

in order to improve the performance of detection of bleed frames, a post-processing operation is performed on the video clip to detect the real bleed zones in the bleed frames on the basis of the post-processing operation. The suggested methods steps will all be explained in the sections that follow. This research was approved by the Institutional review board (IRB) of Ningbo Second Hospital, and a video dataset was collected from arthroscopic surgeries performed at Ningbo Second Hospital, all arthroscopic video data were selected by surgeons, and a detailed description of the video dataset can be found in Pare III.

A. PREPROCESSING

In each frame of arthroscopic videos, the central region retains the most crucial information, thus becoming the focus of this paper. The black area appearing around the central region in each image does not carry any information related to bleeding or non-bleeding. Therefore, the method proposed in this paper, the removal of the black surrounding area the central region of the image is first considered. Subsequently, the further processing is conducted to obtain the final preprocessed images after removing the black areas at the corners. Figure 2 displays the successive outputs showing the removal of the undesirable outside black zones.

B. TRANSFORMATION FROM RGB TO A COMPOSITE PLANE

The RGB color space is the most often utilised of all the color spaces since it is generally accepted that certain shades

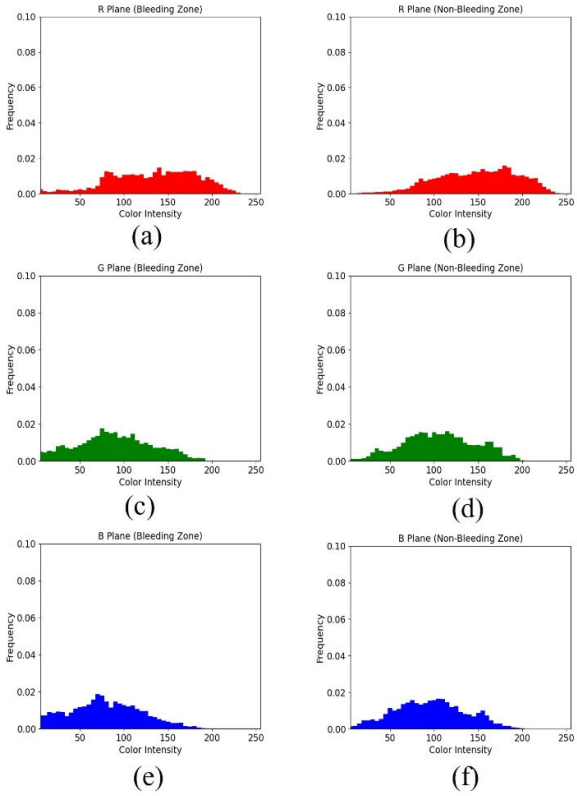

FIGURE 3. The following color plane histograms are created from the bleeding and non-bleeding zones: (a) Red in the bleeding zone; (c) Green in the bleeding zone; (e) Blue in the bleeding zone; (b) Red in the non-bleeding zone; (d) Green in the non-bleeding zone; and (f) Blue in the non-bleeding zone.

of red correspond to the color of blood [21]. Nevertheless, as bleeding zones in arthroscopic images manifest in varying shades of red, direct consideration of RGB intensity values for bleeding zone identification would yield unsatisfactory results. In contrast to capsule endoscopy, illumination in arthroscopic procedures is typically accomplished using a light source and fiber optic system rather than relying on a battery. This approach leads to illumination changes that remain consistently over time. Consequently, there is no need to account for changes in illumination causing intensity deviations in the R, G, and B planes throughout the study. And thus, the continuous light conditions avoided the effect on the intensity deviation between the bleeding and non-bleeding zones. This reduces the unfavourable conditions for the study in this paper. In addition, consistent lighting conditions also help to improve image quality, which makes the detection of bleed zones more reliable. Due to the consistency of the lighting conditions, this provides a more ideal environment for the study in this paper, and by ensuring the consistency of the light source, we will be able to exclude external variables caused by changes in lighting, which makes our detection results more stable and reliable.

The different pixel intensity distributions between the bleeding and non-bleeding zones are examined. Figure 3 displays histograms illustrating intensity levels in the R, G and B planes of arthroscopic video images corresponding

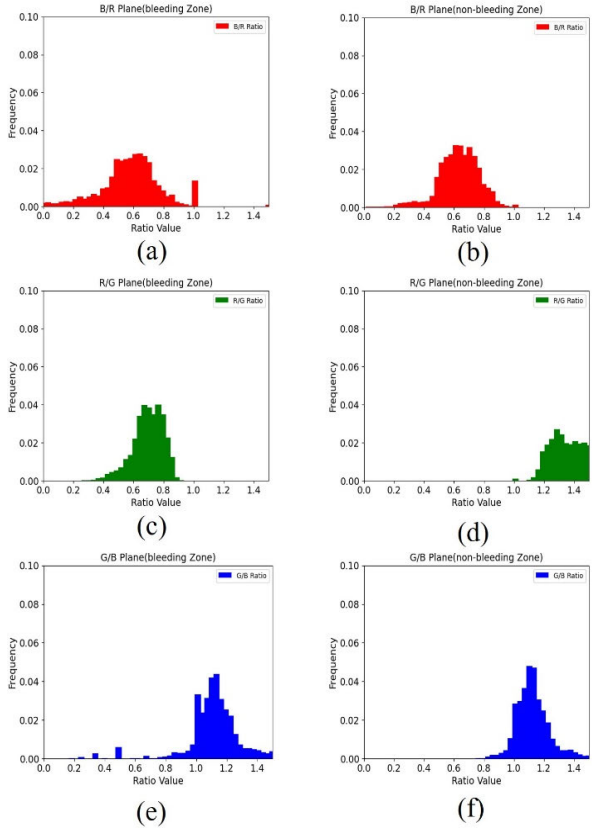

FIGURE 4. Histogram derived from zones of bleeding and non-bleeding in various ratio planes: The bleeding zone is defined as follows: (a) The blue to red ratio (B/R); (c) The red to green ratio (R/G); (e) The green to blue ratio (G/B); (b) The blue to red ratio (B/R) In the non-bleeding zone; (d) The red to green ratio (G/B) In the non-bleeding zone; (f) The green to blue ratio (G/B) In the non-bleeding zone.

with the respective zones. This figure clearly indicates that histograms obtained with a single plane results in a significant overlap between bleeding and non-bleeding categories in arthroscopic video images, posing a considerable challenge to the classification task. This overlap suggests that relying solely on any of the three RGB color planes to distinguish between bleeding and non-bleeding zones is not persuasive enough, as it does not capture that ample information to accurately distinguish those two types of zones.

To further characterize the trend of pixel values, three composite planes B/R, R/G and G/B are evaluated. With these assessments, we hope to find more effective ways to differentiate bleeding and non-bleeding zones. Figure 4 distinctly illustrates the absence of overlaps in red-to-green intensities of bleeding and non-bleeding pixels, which suggests that it is feasible to use red-green intensity ratios to distinguish these two types of zones. While the significant overlaps are observed in the blue-to-red and green-to-blue composite planes. Consequently, this paper employs a composite plane comprising pixel intensity ratios from the red-to-green plane for the features extraction. The R/G composite plane is calculated as:

$$P(x, y) = \frac{R(x, y)}{G(x, y)} \tag{1}$$

TABLE 1. Accuracy obtained for different combinations of features.

Feature combination	Accuracy
Mean+Variance	0.848
Mean+Kurtosis	0.879
Mean+ Variance+ Kurtosis	0.914
Mean+Variance+Skewness	0.926
Mean+Variance+Energy+Entropy	0.937
Mean+Variance+Energy+ Kurtosis+ Skewness	0.942
Mean+Variance+ Skewness+Kurtosis	0.953

where $P(x, y)$ denotes the intensity value of the composite plane at position (x, y) in the image, $R(x, y)$ denotes the intensity value of the red channel at position (x, y) in the image, and $G(x, y)$ denotes the intensity value of the green channel at position (x, y) in the image.

C. EXTRACTING STATISTICAL FEATURES FROM R/G DOMAIN

Under the stable lighting conditions unaffected by temporal changes, this paper does not directly consider the RGB color space, it employs the R/G composite plane instead. With this conversion, we can process the color information in an image more efficiently. By obtaining the statistical features from the image and testing them continuously, the optimal features combination is found, resulting in a more accurate way to distinguish images with and without bleeding. In the process, this paper detailedly analyses the impact of multiple feature combinations on classification accuracy. Table 1 shows the accuracy obtained with the combinations of features selected in this paper, which can be seen from Table 1 that the best accuracy can be achieved by utilizing two low-order and two high-order statistical features for feature extraction, therefore, the mean, variance, skewness and kurtosis are selected for feature extraction in this paper. Mean and variance as low-order statistical features provide basic distributional information; skewness and kurtosis as higher-order statistical features capture the asymmetry and spikiness of the distribution, thus, those features are very helpful in distinguishing bleeding and non-bleeding images.

1) MEAN

For a given collection of values, the mean is their arithmetic average. The mean is defined as the sum of all elements divided by the total number of elements. In the images, the mean is defined as the sum of the pixel intensities divided by the total number of pixels, and it describes the overall brightness or color distribution of the images. If AB was the size of the Arthroscopic image and $I(x, y)$ was the definition of R to G pixel intensity, then the mean would be computed as follows:

$$\bar{I} = \frac{1}{AB} \sum_{x=1}^{A} \sum_{y=1}^{B} I(x, y) \tag{2}$$

2) VARIANCE

Variance constitutes a statistical indicator employed to assess the extent of data dispersion within a dataset. The variance

measures the degree of dispersion of the pixel values, that is the degree of variation in the pixel values. The formula for computing the variance of image intensity is as follows:

$$\sigma^2 = \frac{1}{AB}\sum_{x=1}^{A}\sum_{y=1}^{B}[I(x,y)-\bar{I}]^2 \tag{3}$$

where $\bar{I}$ is the mean defined in equation (2) and $I(x, y)$ is the R to G pixel intensity ratio.

3) SKEWNESS

Skewness is utilized to characterize the asymmetry of data distribution, determining whether the data exhibits a left or right skew. In the context of the images features extraction, Skewness measures the symmetry of the distribution of images pixel values. Skewness is not usually applied directly at the pixel level but is more commonly employed to describe the distribution characteristics of pixel values within a specific region. The definition of skewness is:

$$\gamma = \frac{1}{AB}\sum_{x=1}^{A}\sum_{y=1}^{B}[\frac{I(x,y)-\bar{I}}{\sigma}]^3 \tag{4}$$

where σ is defined as:

$$\sigma = \sqrt{\frac{1}{AB}\sum_{x=1}^{A}\sum_{y=1}^{B}(I(x,y)-\bar{I})^2} \tag{5}$$

where $\bar{I}$ is the mean defined in (2) and $I(x, y)$ is the R to G pixel intensity ratio. σ is the standard deviation of the image.

4) KURTOSIS

Kurtosis is utilized to describe the extent of tail weightiness in a probability distribution or dataset, reflecting the peak characteristics of the data distribution. In the context of images features extraction, kurtosis is not usually applied directly at the pixel level but is employed to characterize the distribution features of pixel values within a specific region. Kurtosis measures the peak state of the distribution of image pixel values, with high kurtosis indicating a steeper distribution and low kurtosis indicating a gentler distribution. The formal definition of kurtosis is as follows:

$$\beta = \frac{1}{AB}\sum_{x=1}^{A}\sum_{y=1}^{B}[\frac{I(x,y)-\bar{I}}{\sigma}]^4 - 3 \tag{6}$$

Nevertheless, in kurtosis calculations, μ_4 is generally employed to ascertain whether the data distribution exhibits greater sharpness or flatness. Hence, kurtosis computations typically utilize the value of μ_4 for representation. This is defined as:

$$\mu_4 = \frac{1}{AB}\sum_{x=1}^{A}\sum_{y=1}^{B}[I(x,y)-\bar{I}]^4 \tag{7}$$

Therefore, according to the fourth central moment, kurtosis is defined as:

$$\beta = \frac{\mu_4}{\sigma^4} \tag{8}$$

where $\bar{I}$ is the mean defined in (2) and $I(x, y)$ is the R to G pixel intensity ratio. μ_4 is the fourth central moment. σ is the standard deviation of the image.

TABLE 2. Feature selection strategy.

Statistical measure	Feature selection condition	Whether to remove
Mean	If $\bar{I} > \theta_{mean}$	No
Variance	If $\sigma^2 < \theta_{\text{var}}$	Yes
Skewness	If $\gamma > \theta_{skew}$	No
Kurtosis	If $\beta < \theta_{kurt}$	Yes

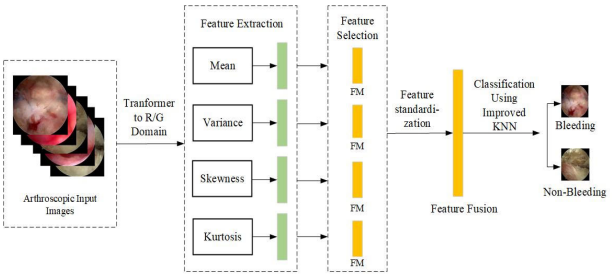

FIGURE 5. Schematic diagram of the proposed method.

D. FEATURE SELECTION

After extracting the four statistical measures of mean, variance, skewness and kurtosis from the images, this paper adopts a simple and fast method, namely the Filter Method(FM), to select the extracted features [22]. First, the thresholds of mean value, variance, skewness and kurtosis are respectively set as $\theta_{mean}, \theta_{var}, \theta_{skew}, \theta_{kurt}$ respectively. These thresholds were selected based on preliminary experimental results and experience.Then, the calculated statistical measures are compared with the set thresholds, For some statistics, if the value exceeded the set threshold, then the feature would be considered to be important in distinguishing bleeding and non-bleeding images and was retained for the subsequent classification process. Conversely, if some statistics did not reach the threshold, the feature would be considered to contribute less to the classification and could be ignored. And the feature selection strategy was as follows:

According to the set threshold conditions, after features selection, some useless features are removed and useful features are retained for the next step of feature fusion. Figure 5 illustrates the process of feature selection and feature fusion.

E. FEATURE FUSION

In order to eliminate the dimensional differences between different features, this paper first uses feature standardization to make them fuse on the same scale. The normalisation rule is as follows, after feature selection, the selected features are combined into a feature vector and then all the feature vectors are combined into a feature matrix X as follows:

$$X = \begin{bmatrix} \bar{I}_1 & \sigma_1^2 & \gamma_1 & \beta_1 \\ \bar{I}_2 & \sigma_2^2 & \gamma_2 & \beta_2 \\ \vdots & \vdots & \vdots & \vdots \\ \bar{I}_n & \sigma_n^2 & \gamma_n & \beta_n \end{bmatrix} \tag{9}$$

Then after calculating the mean and standard deviation of each feature column, each feature is normalised using the

following normalisation formula:

$$x'' = \frac{x - \bar{I}}{\sigma} \tag{10}$$

The normalisation results in a new feature matrix X' as follows:

$$X' = \begin{bmatrix} \bar{I}'_1 & \sigma'^2_1 & \gamma'_1 & \beta'_1 \\ \bar{I}'_2 & \sigma'^2_2 & \gamma'_2 & \beta'_2 \\ \vdots & \vdots & \vdots & \vdots \\ \bar{I}'_n & \sigma'^2_n & \gamma'_n & \beta'_n \end{bmatrix} \tag{11}$$

where μ'' denote the standardised mean, variance, skewness and kurtosis.

After standardizing the features, this paper selects a feature concatenation algorithm to integrate the features together. The feature vector after integration using the feature concatenation algorithm can be expressed as follows:

$$x_{concat} = [\bar{I}'_{1\times n}, \sigma'_{1\times n}, \gamma'_{1\times n}, \beta'_{1\times n}] \tag{12}$$

The features are fused and then used for classification in the next step of the KNN algorithm, which is described in detail in the next section.

F. K-NEAREST NEIGHBOR (KNN) CLASSIFIER

The K-Nearest Neighbors (KNN) classifier is a supervised learning algorithm tailored to address classification problems [23]. Its operational principle is straightforward and intuitive, when encountering an unlabeled data sample, the classifier computes the distance or similarity between the sample and every labeled data point in the dataset. Subsequently, it identifies the K nearest labeled samples. The KNN classifier then ascertains the category of the unlabeled sample by conducting a majority of votes among these K nearest neighbors. When K is set to 1, the sample's category is directly determined by its closest neighbors. In the KNN classifier, identifying an appropriate K value is often crucial for achieving optimal classification performance. In this paper, a KNN improvement algorithm for weighted K nearest neighbours is proposed and the method flow is shown in Figure 6. In the method proposed in this paper, the fused feature vectors are first divided into training and test sets, and then the distance between it and each training sample is calculated for each test sample, and here the distance uses the Euclidean distance [24]. The Euclidean distance is defined as:

$$d = \sqrt{\sum_{i=1}^{n} (x_i - y_i)^2} \tag{13}$$

where n is the number of features, x_i and y_i denote the i-th eigenvalue of the two data points in the feature space respectively.

Subsequently, the nearest k neighbours are selected according to the distance and weight of each neighbour is calculated, next, Next, the weight is voted, the weighted sum of each category is calculated, and the category with the largest weighted sum is assigned to the test sample. Finally, the prediction

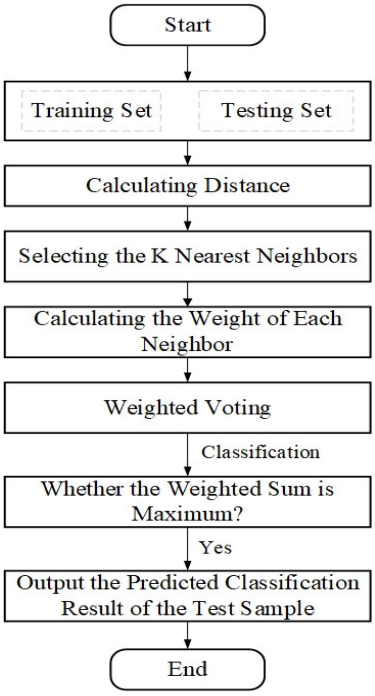

FIGURE 6. Improved KNN algorithm.

and classification results of the test samples are output. This paper calculates the weight of each neighbor using the inverse distance weight, which is defined as:

$$w_i = \frac{1}{d_i} \tag{14}$$

where d_i is the distance to the i-th neighbour.

G. VIDEO POST-PROCESSING

In the preceding section, the KNN classifier was delineated. This work uses a post-processing technique to improve the recognition accuracy after the KNN classifier has classified images as bleeding or non-bleeding. Upon scrutinizing arthroscopic bleeding and non-bleeding videos, we observed that isolated bleeding or non-bleeding frames rarely appear in the videos. To process the test frame, a specific test frame is first selected. Then, based on this frame, the two preceding frames and the two subsequent frames are chosen to form an investigation area. The total size of this investigative area is set to include five frames. Following this, trustworthiness-weighted scores are assigned to each frame, indicating the level of trust or confidence in that frame. Ultimately, these trust scores influence the final decision.The trustworthiness score is defined as:

$$T = w_1 \cdot C + w_2 \cdot D \tag{15}$$

where w_1 is a parameter used to weigh the confidence of the classifier, w_2 is a parameter used to weigh the temporal distance, and $w_1 + w_2 = 1$. C is the confidence score of the classification result provided by the classifier for each frame, the probability value of the classifier output is taken directly as C,and D is calculated based on the temporal distance

between the test frame and the frames in the investigated area.The formula is:

$$D = abs(n_{test} - n_{survey}) \tag{16}$$

where n_{test} is the frame number of the test frame and n_{survey} is the frame number of the frame in the survey area.

The proposed post-processing algorithm is described as follows:

1) For each test frame, trust weighting is performed to assign a trust score to the frame, which represents the degree of trust of the classification results of the frame.

2) When forming the investigation area, consider the trust score and the temporal order of the frames and use the trust score and the temporal order to weight the contribution of each frame in the investigated area.

3) When considering the labels of the majority of frames, frames with higher trust scores are deemed to be more authoritative. Test frame labels should be modified to reflect information of those more authoritative frames if the majority of frames have the opposite labels to the test frame's but those frames with higher trust scores are consistent with the test frame's label.

III. RESULTS AND ANALYSIS

In order to demonstrate how well the suggested method works to identify bleeding frames and bleeding zones in arthroscopy videos, this paper conducts extensive experiments using videos from arthroscopic surgery performed on eight different patients. Four of the videos are annotated as containing bleeding, while the remaining four are labeled as non-bleeding. Expert doctors manually annotated bleeding and non-bleeding images in the videos. The experiment presented bleeding detection results for 2500 arthroscopic video frames, comprising 1850 bleeding frames and 650 non-bleeding frames, all extracted from these eight videos. For classification purposes, K-Nearest Neighbors (KNN) classifiers before and after improvement were used respectively. In KNN classifier, statistical features are first fused and then arthroscopic bleeding and non-bleeding images are classify. To assess the performance of the proposed approach, 80% of the images are randomly selected for training and the remaining 20% of the images are used for testing of the KNN classifier. furthermore a comparison of the suggested method's performance at different K values for the bleeding frame classification was conducted.

A. BLEEDING FRAME DETECTION CRITERIA

To assess the efficacy of the proposed methodology in arthroscopic videos bleeding detection, the criteria for evaluation include accuracy, sensitivity, and specificity [25].The calculation formulas are as follows [26]:

$$Sensitivity = \frac{\sum T_B}{\sum T_B + \sum T_{NB}} \tag{17}$$

$$Specificity = \frac{\sum T_{NB}}{\sum T_{NB} + \sum F_B} \tag{18}$$

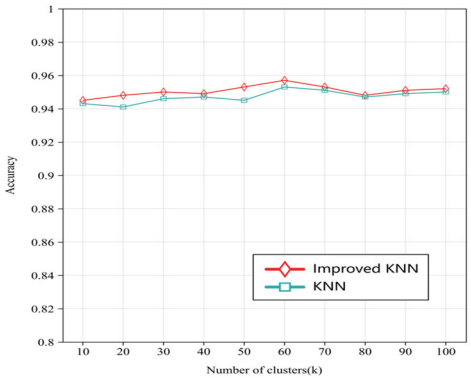

FIGURE 7. Evaluation of bleeding frame recognition accuracy using KNN classifiers before and after improvement and different number of clusters.

$$Accuracy = \frac{\sum T_B + \sum T_{NB}}{\sum T_B + \sum F_{NB} + \sum T_{NB} + \sum F_B} \tag{19}$$

whereas T_B indicates when a bleeding image is correctly detected as a bleeding image; T_{NB} indicates when a non-bleeding image is correctly detected as a non-bleeding image; F_B indicates when a non-bleeding image is mistakenly detected as a bleeding image; and F_{NB} indicates when a bleeding image is mistakenly detected as a non-bleeding image.

Sensitivity is a measure of the accuracy of bleeding frame detection. In the context of bleeding frame detection, sensitivity plays the most critical role because it assesses the test's ability to detect actual bleeding situations, and it is always the primary focus of research in bleeding frame detection. Accuracy reflects the overall correctness of detecting both true bleeding and non-bleeding frames, while specificity indicates the accuracy of identifying non-bleeding images. For these two performance metrics, higher values indicate better performance.

B. BLEEDING FRAME DETECTION

To determine the optimal value of k and evaluate the classification performance of the improved KNN classifier, this paper conducts experiments using both the traditional KNN classifier and the improved KNN classifier. Multiple experiments are conducted with different values of k, ranging from 10 to 100 with intervals of 10, totaling 10 experiments. Figure 7 displays the classification accuracy of arthroscopic video images under different values of k for both the traditional KNN classifier and the improved KNN classifier.

From Figure 7, it is evident that the detection performance is optimal when using the improved KNN classifier with k = 60. Therefore, this paper ultimately selects the improved KNN classifier and conducts experiments on multiple consecutive arthroscopic videos with the k value set to 60.Table 3 below presents the obtained sensitivity, specificity, and accuracy.

In addition to this, In order to test the classification performance under different weights, the weights of and are

TABLE 3. Classification Result With Improved KNN Classifier.

Video name	Accuracy	Sensitivity	Specificity
1	93.7%	95.4%	92.6%
2	95.2%	96.5%	93.3%
3	95.6%	97.1%	94.2%
4	94.5%	96.7%	92.9%

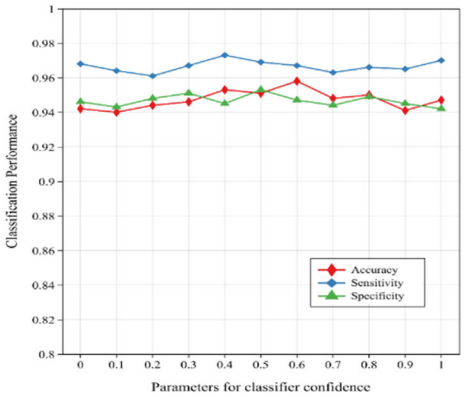

FIGURE 8. Classification performance of classifier confidence and temporal distance under different parameters. X-axis is the classifier confidence parameter.

first determined by a training-based approach, and then the classification performance of the classifier confidence and time distance are tested under different weights. The figure 8 displays the accuracy, sensitivity, and specificity under different weights. Figure 8 illustrates the effective performance of the proposed post-processing scheme in bleeding frame detection. The best classification performance is not achieved when the weight of classifier confidence is set to 0 or 1. The highest classification accuracy of 95.8% is attained when the weight is set to 0.6. This outcome suggests that the post-processing scheme proposed in this paper offers the improved classification of arthroscopic bleeding and non-bleeding images. To assess the effectiveness of the post-processing scheme proposed in this paper for the detection of arthroscopic video bleed frames, the detection performance is compared in both cases without and with post-processing, and the results are presented in Figure 9. The figure reveals that the post-processing scheme proposed in this paper enhances accuracy, sensitivity, and specificity for the detection of bleed frames in arthroscopic videos.

C. BLEEDING ZONE DETECTION

The findings of bleeding zone identification are displayed in this section's Figure 10. The image from the beginning is shown in the first row, and the identified bleed zone is shown in the second one. The images show that the bleeding zone detection used in our suggested approach works effectively.

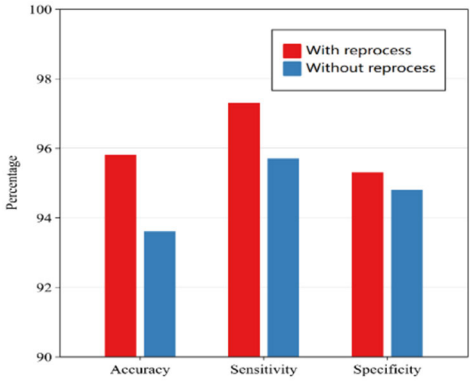

FIGURE 9. Comparison of overall performance with and without reprocess.

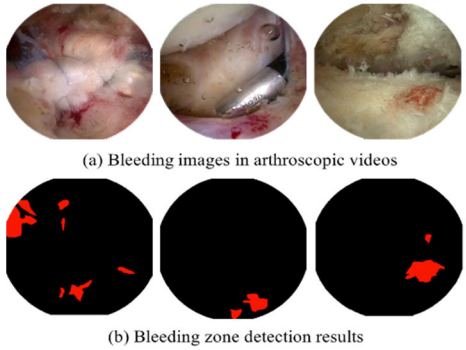

FIGURE 10. Partial bleeding zones detection results.

TABLE 4. Performance comparison of different methods.

Method	Accuracy	Sensitivity	Specificity
Ghosh et.al.[6]	94.42%	—	—
Okamoto et.al.[9]	95%	—	—
Liaqat et.al.[10]	91.92%	82.75%	94.11%
Rain et.al.[17]	95.62%	—	—
Lu et.al.[20]	95.75%	—	—
Ghosh et.al.[21]	93.90%	93.50%	94%
Proposed	**95.8%**	**97.3%**	**95.3%**

D. COMPARISON OF ALGORITHMS

In order to show the performance of the algorithm proposed in this paper in terms of bleeding detection, it is quantitatively compared with the algorithm proposed by Ghosh et al. [6], [21], Okamoto et al. [9], Liaqat et al. [10], Rain et al. [17] and Vajravelu et al. [20]. The comparison results are shown in Table 4. The comparison shows that the algorithm proposed in this paper performs much better in bleeding detection.

IV. DISCUSSION

For the existing arthroscopic surgical process exists in the bleeding easily cause blood mist seriously affect the doctor's field of vision problem. This paper proposes an automatic bleeding visual detection system for arthroscopic video using

composite color and statistical features. The system is able to accurately detect bleeding and identify bleeding zones during surgery, which provides a prerequisite for the doctor to locate and clean the bleeding zone in time and accurately during surgery. This largely reduces the interference of bleeding to the surgeon during surgery, which in turn shortens the surgery time, reduces the difficulty of the surgery, and improves the safety and accuracy of the surgery.

In this paper, the R/G plane is utilized instead of a single plane within the RGB image, and, as depicted in Figure 4, the histogram overlap between the bleeding and non-bleeding zones is nearly zero. Thus, feature extraction within the R/G plane can yield enhanced separation between the bleeding and non-bleeding images. Utilizing different statistical features for extraction within this composite plane maximizes classification accuracy through the application of four statistical measures: mean, variance, skewness and kurtosis. To enhance the classification performance, this paper employs a post-processing algorithm, effectively enhancing the classification accuracy of the system. Finally, to detect bleeding zones, this paper proposes a region-based detection algorithm for identifying bleeding zones in the images.

The experimental results demonstrate that employing the post-processing algorithm for classifying bleeding and non-bleeding images achieved an accuracy of 95.8%, surpassing the performance without post-processing by 2.2%; the sensitivity reached 97.3%, an improvement of 1.5%; and the specificity reached 95.3%, a gain of 0.5%. This suggests that the post-processing algorithm proposed in this paper can significantly enhance the classification performance. Furthermore, the region detection algorithm proposed in this paper also yields satisfactory results for bleeding zone detection. However, while presenting the advantages of the system for bleed detection in arthroscopic images, it is important to recognise the limitations of this study. Because the human joint is an extremely complex and diverse structure, although the system has demonstrated good performance, its performance under different arthroscopic surgical sites remains an area for further research. Therefore, one of the biggest limitations is whether the system remains versatile under arthroscopic surgery at different sites. In addition to this, bleeding during surgery is influenced by a number of factors, including the patient's age, gender, physical condition and surgical site. All of these individualised factors can lead to different situations during surgery, and it is clear that the system proposed in this paper cannot cover all situations. Since most of the research data in this paper were derived from specific joint sites, this may lead to a lack of diversity in the data. Therefore, in future studies, in addition to incorporating all possible influencing factors into the optimisation of the system parameters to establish a more comprehensive bleeding detection system for arthroscopic surgery, the ability of the system to detect bleeding under different types of joint images should also be verified.

V. CONCLUSION

This paper presents a method for detecting bleed frames and bleed zones in arthroscopic videos. Extensive experimental studies have demonstrated that the proposed method achieves high performance in terms of sensitivity, specificity, and accuracy. Rather than directly utilizing the RGB color space inherent to the image, the proposed method extracts features from a given arthroscopic image by employing the red-green intensity ratio as a composite plane, subsequently using different statistical features within this composite plane. To enhance the accuracy of classifying bleeding and non-bleeding images, the post-processing algorithm proposed in this paper significantly improves the detection performance of bleeding frames. Additionally, the automatic detection of bleeding zones proposed in this paper also achieves satisfactory results for localizing the bleeding zones. Thus, the scheme proposed in this paper holds promise in identifying bleeding frames and detecting bleed zones from arthroscopic videos.

This paper has contributed insights into bleeding detection during arthroscopic surgery. Future researches could explore further avenues to improve the accuracy of bleeding detection during arthroscopic surgery based on this study's findings. Simultaneously, efforts are being made to consider multiple individualized influences to enhance the system's robustness and reliability in diverse complex surgical scenarios. In conclusion, this paper provides valuable insights into identifying bleeding during arthroscopic surgery, serving as a useful reference for surgeons to make accurate judgments during surgery, thereby enhancing surgical safety. Additionally, it indirectly assists surgeons in bleeding control and treatment decision-making, thereby potentially improving the success rate of surgical treatments and patients recovery.

REFERENCES

[1] S. Charfi and M. E. Ansari, "Gastrointestinal tract bleeding detection from wireless capsule endoscopy videos," in *Proc. 2nd Int. Conf. Internet Things, Data Cloud Comput.*, Mar. 2017, pp. 1–5, doi: 10.1145/3018896.3025159.

[2] H. S. Pannu, S. Ahuja, N. Dang, S. Soni, and A. K. Malhi, "Deep learning based image classification for intestinal hemorrhage," *Multimedia Tools Appl.*, vol. 79, nos. 29–30, pp. 21941–21966, Aug. 2020, doi: 10.1007/s11042-020-08905-7.

[3] A. Garcia-Martinez, J. M. Vicente-Samper, and J. M. Sabater-Navarro, "Automatic detection of surgical haemorrhage using computer vision," *Artif. Intell. Med.*, vol. 78, pp. 55–60, May 2017, doi: 10.1016/j.artmed.2017.06.002.

[4] T. Ghosh, S. A. Fattah, and K. A. Wahid, "Automatic computer aided bleeding detection scheme for wireless capsule endoscopy (WCE) video based on higher and lower order statistical features in a composite color," *J. Med. Biol. Eng.*, vol. 38, no. 3, pp. 482–496, Jun. 2018, doi: 10.1007/s40846-017-0318-1.

[5] T. Ghosh, S. A. Fattah, and K. A. Wahid, "CHOBS: Color histogram of block statistics for automatic bleeding detection in wireless capsule endoscopy video," *IEEE J. Translational Eng. Health Med.*, vol. 6, pp. 1–12, 2018, doi: 10.1109/JTEHM.2017.2756034.

[6] T. Ghosh, L. Li, and J. Chakareski, "Effective deep learning for semantic segmentation based bleeding zone detection in capsule endoscopy images," in *Proc. IEEE Int. Conf. Image Process.*, Aug. 2018, pp. 3034–3038, doi: 10.1109/ICIP.2018.8451300.

[7] A. K. Kundu and S. A. Fattah, "Probability density function based modeling of spatial feature variation in capsule endoscopy data for automatic bleeding detection," *Comput. Biol. Med.*, vol. 115, Dec. 2019, Art. no. 103478, doi: 10.1016/j.compbiomed.2019.103478.

[8] K. Pogorelov, S. Suman, F. A. Hussin, A. S. Malik, O. Ostroukhova, M. Riegler, P. Halvorsen, S. Hooi Ho, and K. Goh, "Bleeding detection in wireless capsule endoscopy videos—Color versus texture features," *J. Appl. Clin. Med. Phys.*, vol. 20, no. 8, pp. 141–154, Aug. 2019, doi: 10.1002/acm2.12662.

[9] T. Okamoto, T. Ohnishi, H. Kawahira, O. Dergachyava, P. Jannin, and H. Haneishi, "Real-time identification of blood regions for hemostasis support in laparoscopic surgery," *Signal, Image Video Process.*, vol. 13, no. 2, pp. 405–412, Mar. 2019, doi: 10.1007/s11760-018-1369-7.

[10] A. Liaqat, M. A. Khan, J. H. Shah, M. Sharif, M. Yasmin, and S. L. Fernandes, "Automated ulcer and bleeding classification from WCE images using multiple features fusion and selection," *J. Mech. Med. Biol.*, vol. 18, no. 4, Jun. 2018, Art. no. 1850038, doi: 10.1142/s0219519418500380.

[11] M. Hajabdollahi, R. Esfandiarpoor, P. Khadivi, S. M. R. Soroushmehr, N. Karimi, K. Najarian, and S. Samavi, "Segmentation of bleeding regions in wireless capsule endoscopy for detection of informative frames," *Biomed. Signal Process. Control*, vol. 53, Aug. 2019, Art. no. 101565, doi: 10.1016/j.bspc.2019.101565.

[12] A. Caroppo, P. Siciliano, and A. Leone, "An expert system for lesion detection in wireless capsule endoscopy using transfer learning," *Proc. Comput. Sci.*, vol. 219, pp. 1136–1144, Jan. 2023, doi: 10.1016/j.procs.2023.01.394.

[13] F. Rustam, M. A. Siddique, H. U. R. Siddiqui, S. Ullah, A. Mehmood, I. Ashraf, and G. S. Choi, "Wireless capsule endoscopy bleeding images classification using CNN based model," *IEEE Access*, vol. 9, pp. 33675–33688, 2021, doi: 10.1109/ACCESS.2021.3061592.

[14] M. A. Usman, M. R. Usman, G. B. Satrya, M. A. Khan, C. Politis, N. Philip, and S. Y. Shin, "QI-BRiCE: Quality index for bleeding regions in capsule endoscopy videos," *Comput., Mater. Continua*, vol. 67, no. 2, pp. 1697–1712, 2021, doi: 10.32604/cmc.2021.014696.

[15] S. Rathnamala and S. Jenicka, "Automated bleeding detection in wireless capsule endoscopy images based on color feature extraction from Gaussian mixture model superpixels," *Med. Biol. Eng. Comput.*, vol. 59, no. 4, pp. 969–987, Apr. 2021, doi: 10.1007/s11517-021-02352-8.

[16] A. Caroppo, A. Leone, and P. Siciliano, "Deep transfer learning approaches for bleeding detection in endoscopy images," *Computerized Med. Imag. Graph.*, vol. 88, Mar. 2021, Art. no. 101852, doi: 10.1016/j.compmedimag.2020.101852.

[17] K. Rani, G. Devi, S. Kumar, I. N. Figueiredo, and P. N. Figueiredo, "Classification of wireless capsule endoscopy images for bleeding using deep features fusion," in *Proc. Int. Conf. Electr., Comput., Commun. Mechatronics Eng. (ICECCME)*, Nov. 2022, pp. 1–6, doi: 10.1109/ICECCME55909.2022.9987916.

[18] M. J. Alam, R. B. Rashid, S. A. Fattah, and M. Saquib, "RAt-CapsNet: A deep learning network utilizing attention and regional information for abnormality detection in wireless capsule endoscopy," *IEEE J. Transl. Eng. Health Med.*, vol. 10, pp. 1–8, 2022, doi: 10.1109/JTEHM.2022.3198819.

[19] F. Lu, W. Li, S. Lin, C. Peng, Z. Wang, B. Qian, R. Ranjan, H. Jin, and A. Y. Zomaya, "Multi-scale features fusion for the detection of tiny bleeding in wireless capsule endoscopy images," *ACM Trans. Internet Things*, vol. 3, no. 1, pp. 1–19, Feb. 2022, doi: 10.1145/3477540.

[20] A. Vajravelu, K. S. T. Selvan, M. M. B. A. Jamil, A. Jude, and I. D. L. T. Diez, "Machine learning techniques to detect bleeding frame and area in wireless capsule endoscopy video," *J. Intell. Fuzzy Syst.*, vol. 44, no. 1, pp. 353–364, Jan. 2023, doi: 10.3233/jifs-213099.

[21] T. Ghosh, S. A. Fattah, S. K. Bashar, C. Shahnaz, K. A. Wahid, W.-P. Zhu, and M. O. Ahmad, "An automatic bleeding detection technique in wireless capsule endoscopy from region of interest," in *Proc. IEEE Int. Conf. Digit. Signal Process. (DSP)*, Jul. 2015, pp. 1293–1297, doi: 10.1109/ICDSP.2015.7252090.

[22] A. Bommert, X. Sun, B. Bischl, J. Rahnenführer, and M. Lang, "Benchmark for filter methods for feature selection in high-dimensional classification data," *Comput. Statist. Data Anal.*, vol. 143, Mar. 2020, Art. no. 106839, doi: 10.1016/j.csda.2019.106839.

[23] Z. Zhang, "Introduction to machine learning: K-nearest neighbors," *Ann. Transl. Med.*, vol. 4, no. 11, p. 218, Jun. 2016, doi: 10.21037/atm.2016.03.37.

[24] L. Liberti, C. Lavor, N. Maculan, and A. Mucherino, "Euclidean distance geometry and applications," *SIAM Rev.*, vol. 56, no. 1, pp. 3–69, Jan. 2014, doi: 10.1137/120875909.

[25] D. G. Altman and J. M. Bland, "Statistics notes: Diagnostic tests 1: Sensitivity and specificity," *BMJ*, vol. 308, no. 6943, p. 1552, Jun. 1994, doi: 10.1136/bmj.308.6943.1552.

[26] G. Pan, G. Yan, X. Qiu, and J. Cui, "Bleeding detection in wireless capsule endoscopy based on probabilistic neural network," *J. Med. Syst.*, vol. 35, no. 6, pp. 1477–1484, Dec. 2011, doi: 10.1007/s10916-009-9424-0.

ZEWEN LIU is currently pursuing the M.S. degree with the College of Science and Technology, Ningbo University, Ningbo, China. His research interests include computer vision and image processing.

XIANCHENG WANG received the B.S. and M.S. degrees from Harbin Institute of Technology, Harbin, China, in 2002 and 2004, respectively, and the Ph.D. degree from Zhejiang University, Zhejiang, in 2020. He is currently the Vice President of the Institute of Applied Technology, College of Science and Technology, Ningbo University. His research interests include intelligent robot and control, machine vision inspection, and image processing.

YI YUAN received the B.S. and M.S. degrees from Zhejiang University School of Medicine, Zhejiang, China, in 2002 and 2013, respectively. He is currently the Deputy Director of the Department of Joint Surgery and Sports Medicine, The Second Hospital of Ningbo. His research interests include joint surgery and sports medicine. He is a Youth Member of the Upper Limb Group, Sports Medicine Branch, Chinese Medical Association, and the Standing Committee of the Sports Medicine Branch of Zhejiang Medical Association.

RUIDONG LI is currently pursuing the M.S. degree with the College of Science and Technology, Ningbo University, Ningbo, China. His research interests include machine learning and intelligent manufacturing.

WENPING XIANG is currently pursuing the M.S. degree with the College of Science and Technology, Ningbo University, Ningbo, China. His research interests include digital twin and intelligent manufacturing.